Expanded View Figures

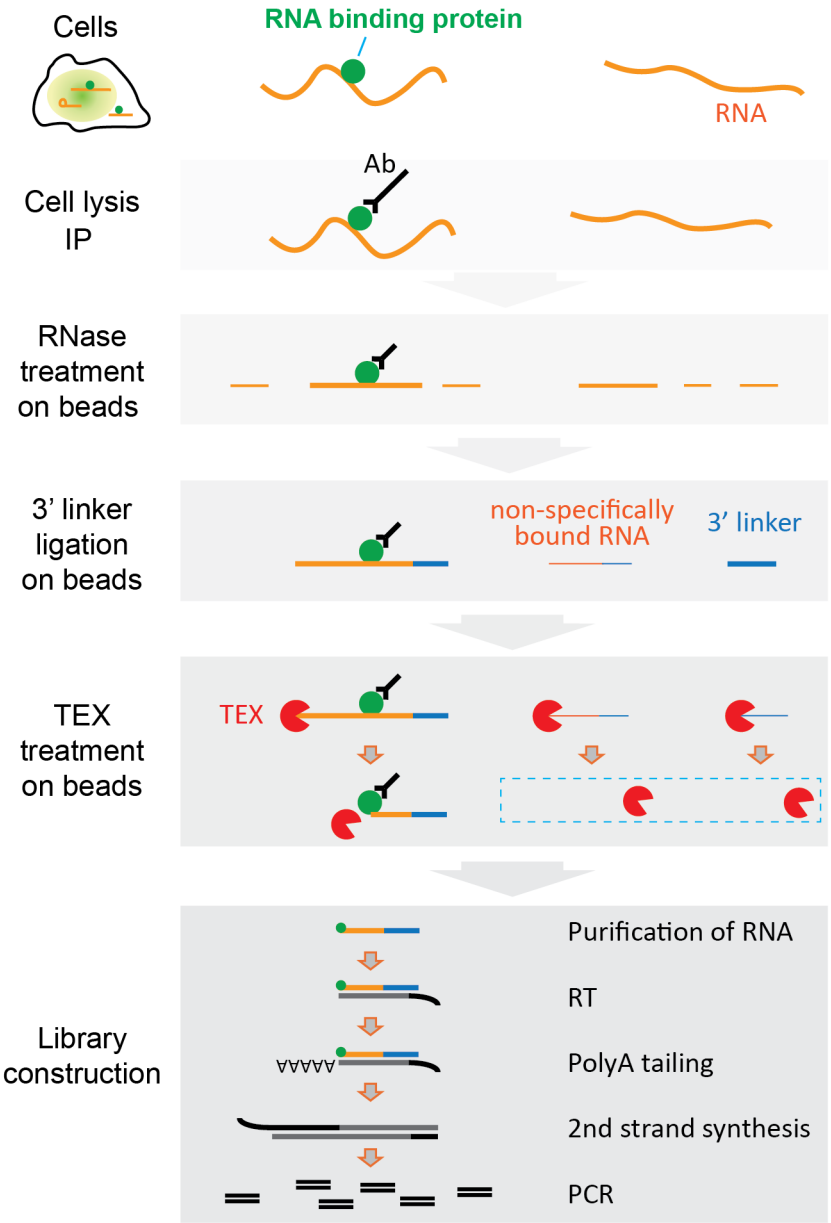

Figure EV1. Schematic representation of the tRIP workflow.
RNA-binding protein (RBP)–RNA complex is immunoprecipitated with an antibody against the RBP. Then, the immunoprecipitated RNA is partially digested with RNase on beads. After stringent washes, a 64-nt linker is ligated to the 3′ end of the RNA fragment, and immunoprecipitants are treated with TEX to eliminate non-specifically remaining RNA and free linkers. The TEX digests immunoprecipitated RNA up to the RBP-tethered site. The immunoprecipitants are then treated with proteinase K, followed by column purification of RNA. After the first-strand synthesis with reverse transcription, a polyA tail is added to the 3′ end of the first-strand cDNA. After the second-strand synthesis with the tagging primer, the double-strand cDNAs are PCR-amplified and subjected to high-throughput sequencing analysis.

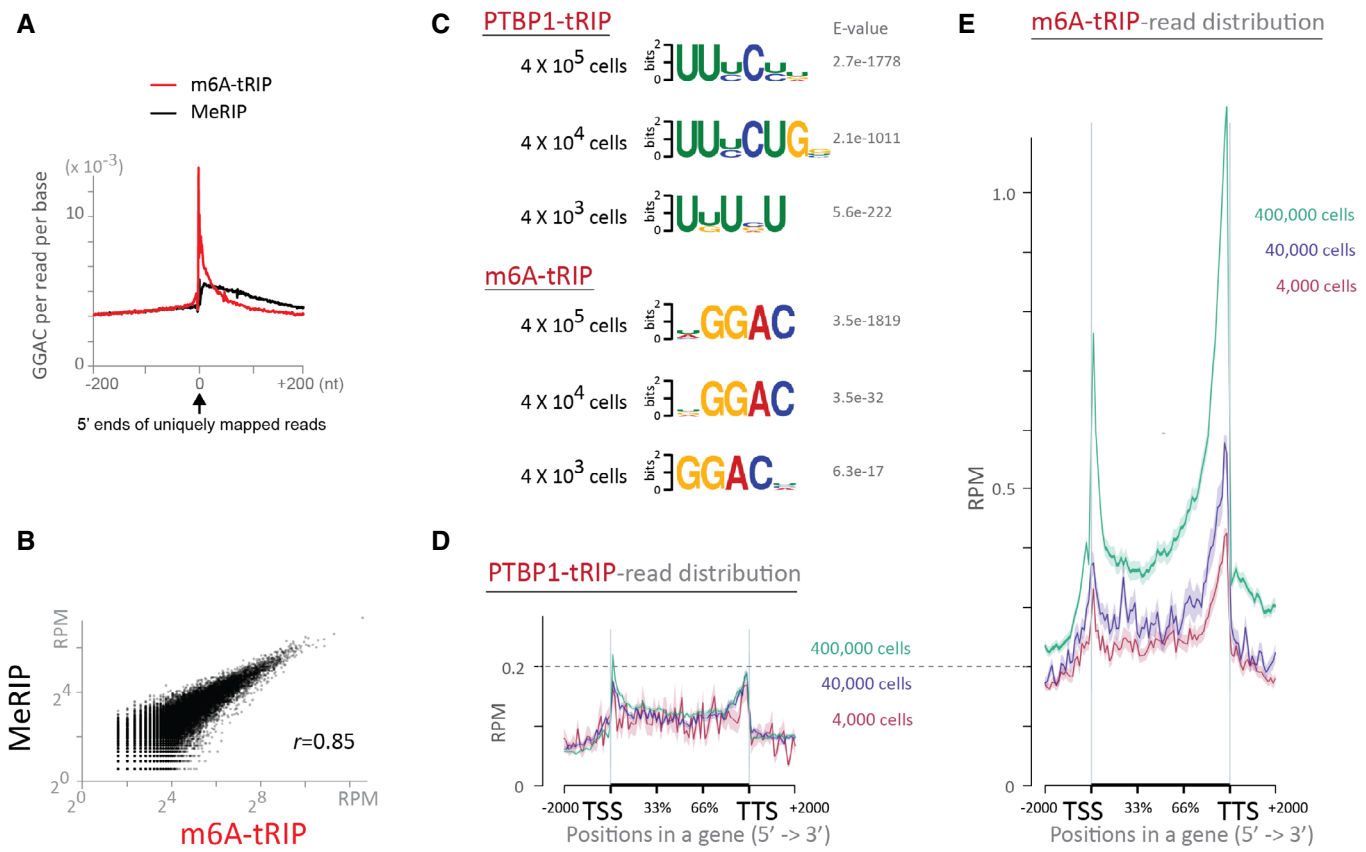

Figure EV2. Read distributions of m6A-tRIP and PTBP1-tRIP.

A The enrichment of m6A motif (GGAC) around the 5′ ends of mapped reads obtained from m6A-tRIP and m6A-MeRIP (RNA-seq of conventional RNA immunoprecipitation using At-m6A antibody).

B Correlation of read densities constituting MACS-defined peaks between m6A-MeRIP and m6A-tRIP. Scatter plot indicates reads per million mapped reads (RPM) of tRIP and MeRIP constituting each peak. Pearson's correlation coefficient (*r*) is indicated.

C The CU-rich PTBP1 motifs (upper panels) and the m6A motifs (lower panels) identified by MEME in the peaks of PTBP1-tRIPs and m6A-tRIPs, respectively, performed using indicated number of C2C12 cells.

D, E Distributions of PTBP1-tRIP reads (D) and m6A-tRIP reads (E) mapped to the relative positions of all mouse coding genes. The ngs.plot tool [58] was used to calculate average RPM on a gene structure. Shown are tRIP-seqs of indicated number of C2C12 cells. The standard error of average RPM is shown as a semi-transparent shade around the average curve.

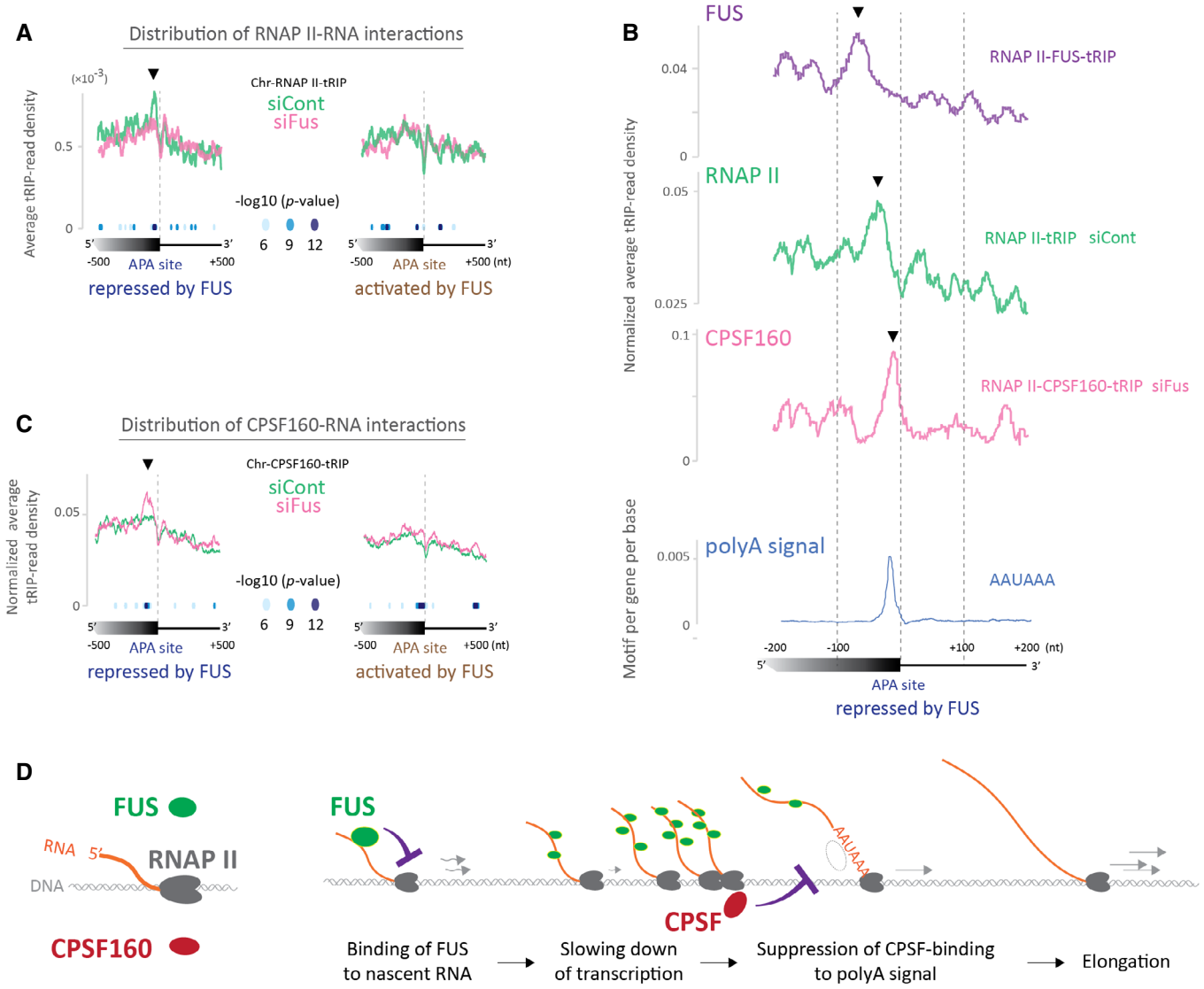

Figure EV3. The recruitment of FUS upstream to polyA sites slows down transcription and inhibits the recognition of polyA signal by CPSF.

A Read distributions of Chr-RNAP II-tRIPs of *Fus*-silenced cells (siFus, pink line) and control siRNA-treated cells (siCont, green line) around APA sites repressed (left graph) or activated (right graph) by FUS. The *P*-values for the differences between siFus and siCont are indicated by circles. An arrowhead indicates a peak upstream to the repressed APA sites detected in Chr-RNAP II-tRIP of siCont-treated cells.

B Expanded view of read distributions of RNAP II-FUS-tRIP (Fig 2E, bold purple line), RNAP II-tRIP of siCont-treated cells (Fig EV3A, green line), and RNAP II-CPSF160-tRIP of *Fus*-silenced cells (Fig 2F, pink line) around FUS-repressed APA sites. The bottom graph shows frequency of the AAUAAA polyadenylation signal (blue line). Arrowheads indicate noticeable peaks detected in the respective tRIP-seqs.

C Read distributions of Chr-CPSF160-tRIPs of *Fus*-silenced cells (siFus, pink line) and control siRNA-treated cells (siCont, green line) around APA sites repressed (left graph) or activated (right graph) by FUS. The *P*-values for the differences between siFus and siCont are indicated by circles. An arrowhead indicates a peak upstream to the repressed APA sites detected in Chr-CPSF160-tRIP of *Fus*-silenced cells.

D A proposed model for FUS-dependent repression of APA. The recruitment of FUS upstream to polyA sites slows down transcription by RNAP II and inhibits the recognition of polyA signal by CPSF, which suppresses subsequent APA and keeps elongation by RNAP II.